Available online at www.sciencedirect.com
ScienceDirect
Journal of Sound and Vibration 319 (2009) 1003–1018
JOURNAL OF SOUND AND VIBRATION
www.elsevier.com/locate/jsvi

Dynamic behavior of triple-walled carbon nanotubes conveying fluid

Y. Yan[a], X.Q. He[b,*], L.X. Zhang[a], C.M. Wang[c]

[a]*Department of Engineering Mechanics, Kunming University of Science and Technology, Kunming 650051, Yunnan, China*
[b]*Department of Building and Construction, City University of Hong Kong, Tat Chee Avenue, Kowloon, Hong Kong*
[c]*Engineering Science Programme and Department of Civil Engineering, National University of Singapore, Kent Ridge, Singapore 119260, Singapore*

Received 11 April 2007; received in revised form 20 June 2008; accepted 1 July 2008
Handling Editor: J. Lam
Available online 23 August 2008

Abstract

In this study, the instability of triple-walled carbon nanotubes (TWCNTs) conveying fluid is studied based on an Euler–Bernoulli beam model. The van der Waals (vdW) interactions between different carbon nanotubes (CNTs) are taken into account in the analysis, and the Galerkin discretization approach is used to solve the coupled equations of the motions. Numerical simulations show that the interlayer vdW interactions play a significant role in the natural frequencies and the stability of TWCNTs. The critical flow velocities—associated with divergence, restabilization and flutter—are determined. The effects of different inner radius and the value of mode N used in Galerkin discretization on the dynamical behaviors of the fluid-conveyed TWCNTs are also examined in detail. Results reveal that the internal moving fluid plays an important role in the instability of TWCNTs.

1. Introduction

Fluid flows inside carbon nanotubes (CNTs) have become an attractive research topic in recent years, and a great deal of literature has been published on topics such as water flow through CNT junctions [1], the reorientability of water molecules inside CNTs [2], the effects of wall–fluid interactions [3], the static wetting behavior of water on a carbon nanotube surface [4], the diffusive transport of light gases in CNTs [5] and the dependence of the fluid behavior on the size of CNTs [6].

In the aforementioned studies, molecular dynamics simulations (MDSs) are involved; however, MDS is complex and time consuming, especially for a large-sized atomic system, due to the limitations of the current computing capacity. Considering the difficulties of a controlled experiment on such a scale, a theoretical simulation seems a better way to investigate the properties of CNTs. It is reported that continuum mechanics models are rather effective in the prediction of the mechanical characteristics of not only single-walled carbon

*Corresponding author.
E-mail address: bcxqhe@cityu.edu.hk (X.Q. He).

0022-460X/$ - see front matter © 2008 Published by Elsevier Ltd.
doi:10.1016/j.jsv.2008.07.001

nanotubes (SWCNTs) but also multi-walled carbon nanotubes (MWCNTs). For example, the equations of a thin hollow cylinder have been applied to analyze the low-frequency vibration of a SWCNT [7], and the prediction of the breathing mode is validated by experiments [8]. Sound velocity predicted by the Euler-beam model agrees well with data obtained by other methods [9]. Buckling and vibrational behaviors of CNTs have also been investigated by using the Euler- and Timoshenko-beam models; moreover, the buckling load, the resonant frequencies and the vibrational modes of SWCNTs are in general agreement with the experimental results [10–12]. In addition, *in-situ* experimental studies have indicated that the liquid behavior in hydrothermal CNTs can be described using continuum fluid transport and phase change concepts except for the extreme case of thin channels and thin liquid films [13]. Furthermore, the water flow measurement through CNTs with diameters of <2 nm was carried out [14]. The results show that in this size regime (about 6 water molecules in diameter) the measured water flow exceeds values calculated from continuum hydrodynamics models by more than three orders of magnitude, because continuum theory concepts such as a velocity profile may be different to be defined. They also reveal that the small differences in nanotube diameter can have large effects on transport. Besides, MDS was used to test the validity of Navier–Stokes equations in analysis of nanochannels [15–19]. The results show that when the fluid flows in slit channels as narrow as 10 fluid molecular diameters, the deviation between the continuum and MDS predictions is very small [19].

Recently, the influence of the internal moving fluid on the free vibration and flow-induced instability of SWCNTs has been studied by modeling the CNT as an Euler–Bernoulli beam [20,21]. The model of Euler–Bernoulli beam gives simply general formulas in many important cases [20–24], which clearly indicate major factors affecting mechanical behaviors of CNTs (and thus rule out other less important parameters). Usually, it is hard to obtain such simple formulas by other methods. It is true that the application of Euler–Bernoulli beam model may not be a best choose for enough short nanotubes compared with shell model [25] and Timshenko-beam model, but because it is simpler and can well predict mainly the physical phenomena. In most cases, we can well predict the bifurcations of the system with the Euler–Bernoulli model as like with the shell model in Ref. [26].

So, in this paper, CNTs are modeled as Euler–Bernoulli beam, and the established governing equations are coupled each other on the basis of a more refined van der Waals (vdW) model [27]. It is noted that the equations of motion for SWCNTs cannot be used directly for TWCNTs due to the vdW interactions between any two different tubes, the governing equations for the vibration and structural instability of a TWCNT conveying fluid are derived herein by using Hamilton's principle. Then, the flow-induced instability and bifurcations of TWCNTs are investigated in detail. In particular, the critical flow velocities are determined for the divergence and flutter of CNTs for the various inner radius and the value of mode N used in the Galerkin discretization. More importantly, the effects of the vdW interactions on the critical velocities and the natural frequencies of the fluid-conveyed TWCNTs are examined.

2. Coupled beam model for TWCNT conveying fluid

The TWCNTs are modeled as a triple-tube pipe which consists of the inner tube of radius R_1, middle tube of radius R_2 and the outer tube of radius R_3 as shown in Fig. 1. The thickness of every tube is h, the length is L, and modulus of elasticity is E. The internal fluid of mass per unit length m_f is assumed to flow steadily through the inner tube with a constant velocity U. The formulation presented here is based on the Euler–Bernoulli beam theory, which leads to the following displacement:

$$\bar{u}_i(x,z,t) = u_i(x,t) - z\frac{\partial w_i}{\partial x},$$

$$\bar{w}_i(x,z,t) = w_i(x,t), \tag{1}$$

where x is the axial coordinate, t is time, $\bar{u}_i$ and $\bar{w}_i$ are the total displacements of the ith tube along the coordinate directions x and z, u_i and w_i denote the axial and transverse displacements of the ith tube on the neutral axis, and the subscript $i = 1, 2, 3$.

The potential energy Π stored in a TWCNT and the virtual kinetic energy T in the TWCNT as well as the fluid inside the TWCNT are given, respectively, by

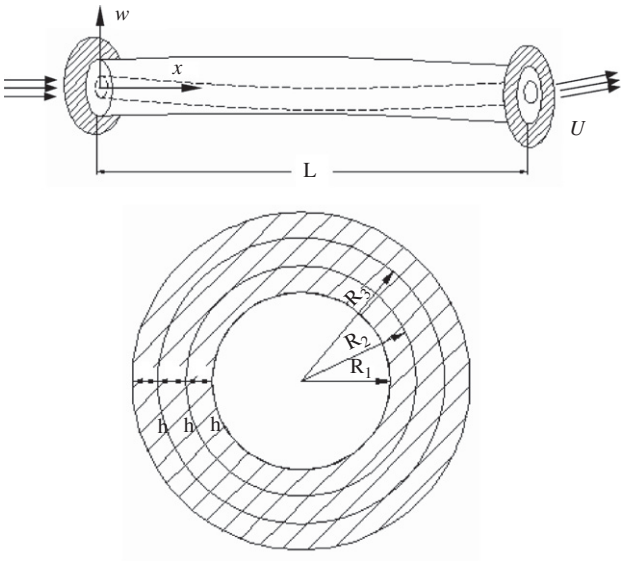

Fig. 1. Clamped TWCNTs conveying fluid of the mass m_f (per unit axial length) at the flow velocity U.

$$\Pi = \frac{E}{2}\int_0^L \left[\int_{A_1} \left(\frac{\partial u_1}{\partial x} - z\frac{\partial^2 w_1}{\partial x^2} \right)^2 \mathrm{d}A + \int_{A_2} \left(\frac{\partial u_2}{\partial x} - z\frac{\partial^2 w_2}{\partial x^2} \right)^2 \mathrm{d}A + \int_{A_3} \left(\frac{\partial u_3}{\partial x} - z\frac{\partial^2 w_3}{\partial x^2} \right)^2 \mathrm{d}A \right] \mathrm{d}x, \tag{2a}$$

$$\begin{aligned} T = {} & \frac{\rho_t}{2}\int_0^L \int_{A_1} \left[\left(\frac{\partial u_1}{\partial t} - z\frac{\partial \dot{w}_1}{\partial x} \right)^2 + \left(\frac{\partial w_1}{\partial t} \right)^2 \right] \mathrm{d}A\,\mathrm{d}x \\ & + \frac{\rho_t}{2}\int_0^L \int_{A_2} \left[\left(\frac{\partial u_2}{\partial t} - z\frac{\partial \dot{w}_2}{\partial x} \right)^2 + \left(\frac{\partial w_2}{\partial t} \right)^2 \right] \mathrm{d}A\,\mathrm{d}x \\ & + \frac{\rho_t}{2}\int_0^L \int_{A_3} \left[\left(\frac{\partial u_3}{\partial t} - z\frac{\partial \dot{w}_3}{\partial x} \right)^2 + \left(\frac{\partial w_3}{\partial t} \right)^2 \right] \mathrm{d}A\,\mathrm{d}x \\ & + \int_0^L \int_{A_f} \frac{1}{2}\rho_f \left[\left(\frac{\partial u_1}{\partial t} + U\cos\theta_1 \right)^2 + \left(\frac{\partial w_1}{\partial t} - U\sin\theta_1 \right)^2 + z^2 \left(\frac{\partial^2 w_1}{\partial x\,\partial t} \right)^2 \right] \mathrm{d}A\,\mathrm{d}x, \end{aligned} \tag{2b}$$

where $\theta_1 = -\partial w_1/\partial x$, I_i and m_i are the moment of inertia and the mass of the ith tube per unit length, ρ_t is the mass density of the beam material, ρ_f is the mass density of the fluid inside the tube 1, $A_1 = \pi((R_1+h)^2 - R_1^2)$, $A_2 = \pi((R_2+h)^2 - R_2^2)$ and $A_3 = \pi((R_3+h)^2 - R_3^2)$ are corresponding to the cross-sectional areas of tube 1, tube 2 and tube 3, and $A_f = \pi R_1^2$ is the cross-sectional areas of the fluid passage in tube 1. The subscripts 1, 2, and 3 denote the inner tube, the middle tube and the outer tube, respectively. Thus, the variational form of the equations of the motion for the TWCNTs can be written, by using Hamilton's principle, as

$$\int_{t_0}^{t_1} (\delta\Pi - \delta T - \delta V)\,\mathrm{d}t = 0, \tag{3}$$

where

$$\begin{aligned} \delta\Pi = {} & -EA_1\int_0^L \frac{\partial^2 u_1}{\partial x^2}\,\mathrm{d}x\,\delta u_1 - EA_2\int_0^L \frac{\partial^2 u_2}{\partial x^2}\,\mathrm{d}x\,\delta u_2 - EA_3\int_0^L \frac{\partial^2 u_3}{\partial x^2}\,\mathrm{d}x\,\delta u_3 \\ & + EI_1\int_0^L \frac{\partial^4 w_1}{\partial x^4}\,\mathrm{d}x\,\delta w_1 + EI_2\int_0^L \frac{\partial^4 w_2}{\partial x^4}\,\mathrm{d}x\,\delta w_2 + EI_3\int_0^L \frac{\partial^4 w_3}{\partial x^4}\,\mathrm{d}x\,\delta w_3, \end{aligned} \tag{4a}$$

$$\begin{aligned}\delta T = & -\int_0^L \left((m_1+m_f)\frac{\partial^2 u_1}{\partial t^2}+m_f U\sin\theta_1\frac{\partial^2 w_1}{\partial x\,\partial t}\right)\mathrm{d}x\,\delta u_1 - m_2\int_0^L \frac{\partial^2 u_2}{\partial t^2}\,\mathrm{d}x\,\delta u_2 - m_2\int_0^L \frac{\partial^2 w_2}{\partial t^2}\,\mathrm{d}x\,\delta w_2\\ & - m_3\int_0^L \frac{\partial^2 u_3}{\partial t^2}\,\mathrm{d}x\,\delta u_3 - m_3\int_0^L \frac{\partial^2 w_3}{\partial t^2}\,\mathrm{d}x\,\delta w_3 - \int_0^L (m_1+m_f)\frac{\partial^2 w_1}{\partial t^2}\,\mathrm{d}x\,\delta w_1\\ & + (\rho_t I_1+\rho_f I_f)\int_0^L \frac{\partial^4 w_1}{\partial x^2\,\partial t^2}\,\mathrm{d}x\,\delta w_1 + \rho_t I_2\int_0^L \frac{\partial^4 w_2}{\partial x^2\,\partial t^2}\,\mathrm{d}x\,\delta w_2 + \rho_t I_3\int_0^L \frac{\partial^4 w_3}{\partial x^2\,\partial t^2}\,\mathrm{d}x\,\delta w_3\\ & + m_f\left[\int_0^L\left(-U\sin\theta_1\frac{\partial^2 u_1}{\partial x\,\partial t}+\frac{\partial u_1}{\partial t}U\cos\theta_1\frac{\partial^2 w_1}{\partial x^2}\right)\right]\mathrm{d}x\,\delta w_1\\ & + m_f\int_0^L\left[\left(-U\cos\theta_1\frac{\partial^2 w_1}{\partial x\,\partial t}-\frac{\partial w_1}{\partial t}U\sin\theta_1\frac{\partial^2 w_1}{\partial x^2}-U\cos\theta_1\frac{\partial^2 w_1}{\partial x\,\partial t}\right)\right]\mathrm{d}x\,\delta w_1, \end{aligned} \tag{4b}$$

and the virtual work due to the vdW interactions and the interactions between tube 1 and the flowing fluid:

$$\begin{aligned}\delta V = & \int_0^L\left[c_{12}(w_1-w_2)+c_{13}(w_1-w_3)-m_f U^2\frac{\partial^2 w_1}{\partial x^2}\cos\theta_1\right]\mathrm{d}x\,\delta w_1\\ & + \int_0^L [c_{21}(w_2-w_1)+c_{23}(w_2-w_3)]\,\mathrm{d}x\,\delta w_2\\ & + \int_0^L [c_{31}(w_3-w_1)+c_{32}(w_3-w_2)]\,\mathrm{d}x\,\delta w_3\\ & - \int_0^L m_f U^2\frac{\partial^2 w_1}{\partial x^2}\sin\theta_1\,\mathrm{d}x\,\delta u_1, \end{aligned} \tag{4c}$$

where all the terms involving $[\cdot]_0^L$ and $[\cdot]_{t_0}^{t_1}$ vanish on account of the clamped ends and the assumption that all variables and derivatives are zero at $t=t_0$ and t_1, and c_{ij} is the vdW interaction coefficient which can be expressed as [27]

$$c_{ij} = -2\left[\frac{1001\pi\varepsilon\sigma^{12}}{3a^4}E_{ij}^{13} - \frac{1120\pi\varepsilon\sigma^6}{9a^4}E_{ij}^{7}\right]R_i R_j, \tag{5a}$$

where ε, a and σ are the parameters used in calculating the vdW interaction coefficient [28], and

$$E_{ij}^m = (R_i+R_j)^{-m}\int_0^{\pi/2}\frac{\mathrm{d}\theta}{[1-K_{ij}\cos^2\theta]^{m/2}}, \tag{5b}$$

$$K_{ij} = \frac{4R_iR_j}{(R_i+R_j)^2}. \tag{5c}$$

We assume that $\theta_i = -\partial w_i/\partial x$ is small such that $\cos\theta_i \approx 1$ and $\sin\theta_i \approx \theta_i$. Substituting for $\delta\Pi, \delta T$ and δV from Eqs. (4a)–(4c) into Eq. (3), we obtain the governing equations for the vibration and structural instability of the TWCNTs conveying fluid:

$$(m_1+m_f)\frac{\partial^2 u_1}{\partial t^2} - m_f U\frac{\partial w_1}{\partial x}\frac{\partial^2 w_1}{\partial x\,\partial t} - EA_1\frac{\partial^2 u_1}{\partial x^2} - m_f U^2\frac{\partial^2 w_1}{\partial x^2}\frac{\partial w_1}{\partial x} = 0, \tag{6a}$$

$$m_2\frac{\partial^2 u_2}{\partial t^2} - EA_2\frac{\partial^2 u_2}{\partial x^2} = 0, \tag{6b}$$

$$(m_f+m_1)\frac{\partial^2 w_1}{\partial t^2}-(\rho_t I_1+\rho_f I_f)\frac{\partial^4 w_1}{\partial x^2\,\partial t^2}-m_f U\left(\frac{\partial w_1}{\partial x}\frac{\partial^2 u_1}{\partial x\,\partial t}+\frac{\partial u_1}{\partial t}\frac{\partial^2 w_1}{\partial x^2}\right)+EI_1\frac{\partial^4 w_1}{\partial x^4}$$
$$+m_f U^2\frac{\partial^2 w_1}{\partial x^2}+2m_f U\frac{\partial^2 w_1}{\partial x\,\partial t}-m_f U\frac{\partial w_1}{\partial t}\frac{\partial w_1}{\partial x}\frac{\partial^2 w_1}{\partial x^2}=c_{12}(w_1-w_2)+c_{13}(w_1-w_3), \tag{6c}$$

$$EI_2\frac{\partial^4 w_2}{\partial x^4}+m_2\frac{\partial^2 w_2}{\partial t^2}-\rho_t I_2\frac{\partial^4 w_2}{\partial x^2\,\partial t^2}=c_{21}(w_2-w_1)+c_{23}(w_2-w_3), \tag{6d}$$

$$m_3\frac{\partial^2 u_3}{\partial t^2}-EA_3\frac{\partial^2 u_3}{\partial x^2}=0, \tag{6e}$$

$$EI_3\frac{\partial^4 w_3}{\partial x^4}+m_3\frac{\partial^2 w_3}{\partial t^2}-\rho_t I_3\frac{\partial^4 w_3}{\partial x^2\,\partial t^2}=c_{31}(w_3-w_1)+c_{32}(w_3-w_2). \tag{6f}$$

Consider the case of the TWCNTs with clamped ends. The boundary conditions are $w=0$ and $\partial w/\partial x=0$ at both ends. It is noted that there are no tangential external loading along the axial or the circumferential directions of the TWCNTs. In this case, the deformation of the TWCNTs along the axial direction can be neglected and the equations of the motion for the radial deflection w_i of the ith tube of the TWCNTs can be simplified, by omitting all of the nonlinear terms and fourth derivative with respect to time and spatial. Three coupled equations, thus, are obtained as

$$(m_f+m_1)\frac{\partial^2 w_1}{\partial t^2}+EI_1\frac{\partial^4 w_1}{\partial x^4}+m_f U^2\frac{\partial^2 w_1}{\partial x^2}+2m_f U\frac{\partial^2 w_1}{\partial x\,\partial t}=c_{12}(w_1-w_2)+c_{13}(w_1-w_3), \tag{7a}$$

$$EI_2\frac{\partial^4 w_2}{\partial x^4}+m_2\frac{\partial^2 w_2}{\partial t^2}=c_{21}(w_2-w_1)+c_{23}(w_2-w_3), \tag{7b}$$

$$EI_3\frac{\partial^4 w_3}{\partial x^4}+m_3\frac{\partial^2 w_3}{\partial t^2}=c_{31}(w_3-w_1)+c_{32}(w_3-w_2). \tag{7c}$$

The following dimensionless quantities are used:

$$\xi=\frac{x}{L},\quad \eta_1=\frac{w_1}{L},\quad \eta_2=\frac{w_2}{L},\quad \eta_3=\frac{w_3}{L},\quad \tau=\left[\frac{EI_1}{m_f+m_1}\right]^{1/2}\frac{t}{L^2},\quad u=\left(\frac{m_f}{EI_1}\right)^{1/2}LU,$$

$$\beta_1=\frac{m_f}{m_f+m_1},\quad \beta_2=\frac{m_2 I_1}{(m_f+m_1)I_2},\quad \beta_3=\frac{m_3 I_1}{(m_f+m_1)I_3},$$

$$\bar{c}_{12}=\frac{c_{12}L^4}{EI_1},\quad \bar{c}_{13}=\frac{c_{13}L^4}{EI_1},\quad \bar{c}_{21}=\frac{c_{21}L^4}{EI_2},\quad \bar{c}_{23}=\frac{c_{23}L^4}{EI_2},\quad \bar{c}_{31}=\frac{c_{31}L^4}{EI_3},\quad \bar{c}_{32}=\frac{c_{32}L^4}{EI_3}. \tag{8}$$

Eqs. (7a)–(7c) may be rewritten in dimensionless form as

$$\frac{\partial^4\eta_1}{\partial\xi^4}+u^2\frac{\partial^2\eta_1}{\partial\xi^2}+2\sqrt{\beta_1}\,u\frac{\partial^2\eta_1}{\partial\xi\,\partial\tau}+\frac{\partial^2\eta_1}{\partial\tau^2}-\bar{c}_{12}(\eta_1-\eta_2)-\bar{c}_{13}(\eta_1-\eta_3)=0, \tag{9a}$$

$$\frac{\partial^4\eta_2}{\partial\xi^4}+\beta_2\frac{\partial^2\eta_2}{\partial\tau^2}-\bar{c}_{21}(\eta_2-\eta_1)-\bar{c}_{23}(\eta_2-\eta_3)=0, \tag{9b}$$

$$\frac{\partial^4\eta_3}{\partial\xi^4}+\beta_3\frac{\partial^2\eta_3}{\partial\tau^2}-\bar{c}_{31}(\eta_3-\eta_1)-\bar{c}_{32}(\eta_3-\eta_2)=0. \tag{9c}$$

For TWCNTs of length L as shown in Fig. 1, letting every individual tube have the same end conditions, the deflections of all tubes can be approximated by N-mode Galerkin discretization, namely

$$\eta_1 = \sum_{r=1}^{N} q_r(\tau)\phi_r(\xi), \quad \eta_2 = \sum_{r=1}^{N} q_{r+N}(\tau)\phi_r(\xi), \quad \eta_3 = \sum_{r=1}^{N} q_{r+2N}(\tau)\phi_r(\xi). \tag{10}$$

The substitution of Eq. (10) into Eqs. (9a)–(9c), followed by multiplication with ϕ_s and integration over the domain [0, 1], yields

$$\sum_{r=1}^{N}\{\delta_{sr}\ddot{q}_r + 2\sqrt{\beta_1}b_{sr}u\dot{q}_r + ((\lambda_r^4 - \bar{c}_{12} - \bar{c}_{13})\delta_{sr} + u^2 d_{sr})q_r + \bar{c}_{12}\delta_{sr}q_{r+N} + \bar{c}_{13}\delta_{sr}q_{r+2N}\} = 0, \tag{11a}$$

$$\sum_{r=1}^{N}\{\beta_2\ddot{q}_{r+N} + \bar{c}_{21}q_r + \bar{c}_{23}q_{r+2N} + (\lambda_r^4 - \bar{c}_{21} - \bar{c}_{23})q_{r+N}\}\delta_{sr} = 0, \tag{11b}$$

$$\sum_{r=1}^{N}\{\beta_3\ddot{q}_{r+2N} + \bar{c}_{31}q_r + \bar{c}_{32}q_{r+N} + (\lambda_r^4 - \bar{c}_{31} - \bar{c}_{32})q_{r+2N}\}\delta_{sr} = 0, \quad s = 1, 2, \ldots, N, \tag{11c}$$

where

$$b_{sr} = \int_0^1 \phi_s\phi_r' \,\mathrm{d}\xi = \frac{4\lambda_r^2\lambda_s^2}{\lambda_r^4 - \lambda_s^4}\{(-1)^{r+s} - 1\},$$

$$d_{sr} = \int_0^1 \phi_s\phi_r'' \,\mathrm{d}\xi = \begin{cases} \dfrac{4\lambda_r^2\lambda_s^2}{\lambda_r^4 - \lambda_s^4}(\lambda_r\sigma_r - \lambda_s\sigma_s)\,[(-1)^{r+s} + 1], & s \neq r, \\ \lambda_r\sigma_r(2 - \lambda_r\sigma_r), & s = r. \end{cases}$$

If considering $N = 2$, Eqs. (11a)–(11c) may be converted into 12 first-order differential equations [29]

$$\dot{q}_1 = p_1, \quad \dot{p}_1 = -2\sqrt{\beta_1}b_{12}up_2 - (\lambda_1^4 + u^2 d_{11} - \bar{c}_{12} - \bar{c}_{13})q_1 - \bar{c}_{12}q_3 - \bar{c}_{13}q_5,$$

$$\dot{q}_2 = p_2, \quad \dot{p}_2 = -2\sqrt{\beta_1}b_{21}up_1 - (\lambda_2^4 + u^2 d_{22} - \bar{c}_{12} - \bar{c}_{13})q_2 - \bar{c}_{12}q_4 - \bar{c}_{13}q_6,$$

$$\dot{q}_3 = p_3, \quad \dot{p}_3 = -\frac{\bar{c}_{21}}{\beta_2}q_1 - \frac{(\lambda_1^4 - \bar{c}_{21} - \bar{c}_{23})}{\beta_2}q_3 - \frac{\bar{c}_{23}}{\beta_2}q_5,$$

$$\dot{q}_4 = p_4, \quad \dot{p}_4 = -\frac{\bar{c}_{21}}{\beta_2}q_2 - \frac{(\lambda_2^4 - \bar{c}_{21} - \bar{c}_{23})}{\beta_2}q_4 - \frac{\bar{c}_{23}}{\beta_2}q_6,$$

$$\dot{q}_5 = p_5, \quad \dot{p}_5 = -\frac{\bar{c}_{31}}{\beta_3}q_1 - \frac{\bar{c}_{32}}{\beta_3}q_3 - \frac{(\lambda_1^4 - \bar{c}_{31} - \bar{c}_{32})}{\beta_3}q_5,$$

$$\dot{q}_6 = p_6, \quad \dot{p}_6 = -\frac{\bar{c}_{31}}{\beta_3} q_2 - \frac{\bar{c}_{32}}{\beta_3} q_4 - \frac{(\lambda_2^4 - \bar{c}_{31} - \bar{c}_{32})}{\beta_3} q_6. \tag{12}$$

Eq. (12) is rewritten in a matrix form as follows:

$$\begin{bmatrix} \dot{q}_1 \\ \dot{p}_1 \\ \dot{q}_2 \\ \dot{p}_2 \\ \dot{q}_3 \\ \dot{p}_3 \\ \dot{q}_4 \\ \dot{p}_4 \\ \dot{q}_5 \\ \dot{p}_5 \\ \dot{q}_6 \\ \dot{p}_6 \end{bmatrix} = \begin{bmatrix} 0 & 1 & 0 & 0 & 0 & 0 & 0 & 0 & 0 & 0 & 0 & 0 \\ H_1 & 0 & 0 & -2\sqrt{\beta_1} u b_{12} & -\bar{c}_{12} & 0 & 0 & 0 & -\bar{c}_{13} & 0 & 0 & 0 \\ 0 & 0 & 0 & 1 & 0 & 0 & 0 & 0 & 0 & 0 & 0 & 0 \\ 0 & 2\sqrt{\beta_1} u b_{12} & H_2 & 0 & 0 & 0 & -\bar{c}_{12} & 0 & 0 & 0 & -\bar{c}_{13} & 0 \\ 0 & 0 & 0 & 0 & 0 & 1 & 0 & 0 & 0 & 0 & 0 & 0 \\ -\frac{\bar{c}_{21}}{\beta_2} & 0 & 0 & 0 & H_3 & 0 & 0 & 0 & -\frac{\bar{c}_{23}}{\beta_2} & 0 & 0 & 0 \\ 0 & 0 & 0 & 0 & 0 & 0 & 0 & 1 & 0 & 0 & 0 & 0 \\ 0 & 0 & -\frac{\bar{c}_{21}}{\beta_2} & 0 & 0 & 0 & H_4 & 0 & 0 & 0 & -\frac{\bar{c}_{23}}{\beta_2} & 0 \\ 0 & 0 & 0 & 0 & 0 & 0 & 0 & 0 & 0 & 1 & 0 & 0 \\ -\frac{\bar{c}_{31}}{\beta_3} & 0 & 0 & 0 & -\frac{\bar{c}_{32}}{\beta_3} & 0 & 0 & 0 & H_5 & 0 & 0 & 0 \\ 0 & 0 & 0 & 0 & 0 & 0 & 0 & 0 & 0 & 0 & 0 & 1 \\ 0 & 0 & -\frac{\bar{c}_{31}}{\beta_3} & 0 & 0 & 0 & -\frac{\bar{c}_{32}}{\beta_3} & 0 & 0 & 0 & H_6 & 0 \end{bmatrix} \begin{bmatrix} q_1 \\ p_1 \\ q_2 \\ p_2 \\ q_3 \\ p_3 \\ q_4 \\ p_4 \\ q_5 \\ p_5 \\ q_6 \\ p_6 \end{bmatrix} \tag{13}$$

where

$$H_1 = -(\lambda_1^4 + u^2 d_{11} - \bar{c}_{12} - \bar{c}_{13}), \quad H_2 = -(\lambda_2^4 + u^2 d_{22} - \bar{c}_{12} - \bar{c}_{13}), \quad H_3 = -\frac{1}{\beta_2}(\lambda_1^4 - \bar{c}_{21} - \bar{c}_{23}),$$

$$H_4 = -\frac{1}{\beta_2}(\lambda_2^4 - \bar{c}_{21} - \bar{c}_{23}), \quad H_5 = -\frac{1}{\beta_3}(\lambda_1^4 - \bar{c}_{31} - \bar{c}_{32}), \quad H_6 = -\frac{1}{\beta_3}(\lambda_2^4 - \bar{c}_{31} - \bar{c}_{32}),$$

$$\sigma_r = -\frac{\cos\lambda_r - \cosh\lambda_r}{\sin\lambda_r - \sinh\lambda_r},$$

$$\delta_{sr} = \int_0^1 \phi_s \phi_r \, \mathrm{d}\xi = \begin{cases} 1, & s = r \\ 0, & s \neq r \end{cases} \tag{14}$$

is the Kronecker's delta, and λ_r denotes the rth dimensionless, eigenvalue of the beam, and $\phi'''' = \lambda^4 \phi_r$, where $\lambda_1 = 4.73$, and $\lambda_2 = 7.85$. The notation $[C]$ represents the coefficient matrix of the right-hand side of Eq. (13) from now on for convenience.

If considering $N = 3$, Eqs. (11a)–(11c) may be converted into 18 first-order differential equations [29]:

$$\dot{q}_1 = p_1, \quad \dot{p}_1 = -2\sqrt{\beta_1} b_{12} u p_2 - 2\sqrt{\beta_1} b_{13} u p_3 - (\lambda_1^4 + u^2 d_{11} - \bar{c}_{12} - \bar{c}_{13}) q_1 - u^2 d_{13} q_3 - \bar{c}_{12} q_4 - \bar{c}_{13} q_7,$$

$$\dot{q}_2 = p_2, \quad \dot{p}_2 = -2\sqrt{\beta_1} b_{21} u p_1 - 2\sqrt{\beta_1} b_{23} u p_3 - (\lambda_2^4 + u^2 d_{22} - \bar{c}_{12} - \bar{c}_{13}) q_2 - \bar{c}_{12} q_5 - \bar{c}_{13} q_8,$$

$$\dot{q}_3 = p_3, \quad \dot{p}_3 = -2\sqrt{\beta_1} b_{31} u p_1 - 2\sqrt{\beta_1} b_{32} u p_2 - u^2 d_{31} q_1 - (\lambda_3^4 + u^2 d_{33} - \bar{c}_{12} - \bar{c}_{13}) q_3 - \bar{c}_{12} q_6 - \bar{c}_{13} q_9,$$

$$\dot{q}_4 = p_4, \quad \dot{p}_4 = -\frac{\bar{c}_{21}}{\beta_2} q_1 - \frac{(\lambda_1^4 - \bar{c}_{21} - \bar{c}_{23})}{\beta_2} q_4 - \frac{\bar{c}_{23}}{\beta_2} q_7,$$

$$\dot{q}_5 = p_5, \quad \dot{p}_5 = -\frac{\bar{c}_{21}}{\beta_2} q_2 - \frac{(\lambda_2^4 - \bar{c}_{21} - \bar{c}_{23})}{\beta_2} q_5 - \frac{\bar{c}_{23}}{\beta_2} q_8,$$

$$\dot{q}_6 = p_6, \quad \dot{p}_6 = -\frac{\bar{c}_{21}}{\beta_2} q_3 - \frac{(\lambda_3^4 - \bar{c}_{21} - \bar{c}_{23})}{\beta_2} q_6 - \frac{\bar{c}_{23}}{\beta_2} q_9,$$

$$\dot{q}_7 = p_7, \quad \dot{p}_7 = -\frac{\bar{c}_{31}}{\beta_3} q_1 - \frac{\bar{c}_{32}}{\beta_3} q_4 - \frac{(\lambda_1^4 - \bar{c}_{31} - \bar{c}_{32})}{\beta_3} q_7,$$

$$\dot{q}_8 = p_8, \quad \dot{p}_8 = -\frac{\bar{c}_{31}}{\beta_3} q_2 - \frac{\bar{c}_{32}}{\beta_3} q_5 - \frac{(\lambda_2^4 - \bar{c}_{31} - \bar{c}_{32})}{\beta_3} q_8,$$

$$\dot{q}_9 = p_9, \quad \dot{p}_9 = -\frac{\bar{c}_{31}}{\beta_3} q_3 - \frac{\bar{c}_{32}}{\beta_3} q_6 - \frac{(\lambda_3^4 - \bar{c}_{31} - \bar{c}_{32})}{\beta_3} q_9. \tag{15}$$

Eq. (15) is rewritten in a matrix form as Eq. (13), in which the matrix $[C]$ is

$$\begin{bmatrix}
0 & 1 & 0 & 0 & 0 & 0 & 0 & 0 & 0 & 0 & 0 & 0 & 0 & 0 & 0 & 0 & 0 & 0 \\
H_1 & 0 & 0 & -2\sqrt{\beta_1}ub_{12} & -u^2 d_{13} & 0 & -\bar{c}_{12} & 0 & 0 & 0 & 0 & 0 & -\bar{c}_{13} & 0 & 0 & 0 & 0 & 0 \\
0 & 0 & 0 & 1 & 0 & 0 & 0 & 0 & 0 & 0 & 0 & 0 & 0 & 0 & 0 & 0 & 0 & 0 \\
0 & 2\sqrt{\beta_1}ub_{12} & H_2 & 0 & 0 & -2\sqrt{\beta_1}ub_{23} & 0 & 0 & -\bar{c}_{12} & 0 & 0 & 0 & 0 & 0 & -\bar{c}_{13} & 0 & 0 & 0 \\
0 & 0 & 0 & 0 & 0 & 1 & 0 & 0 & 0 & 0 & 0 & 0 & 0 & 0 & 0 & 0 & 0 & 0 \\
-u^2 d_{31} & 0 & 0 & -2\sqrt{\beta_1}ub_{32} & K_1 & 0 & 0 & 0 & 0 & 0 & -\bar{c}_{12} & 0 & 0 & 0 & 0 & 0 & -\bar{c}_{13} & 0 \\
0 & 0 & 0 & 0 & 0 & 0 & 0 & 1 & 0 & 0 & 0 & 0 & 0 & 0 & 0 & 0 & 0 & 0 \\
-\frac{\bar{c}_{21}}{\beta_2} & 0 & 0 & 0 & 0 & 0 & H_3 & 0 & 0 & 0 & 0 & 0 & -\frac{\bar{c}_{23}}{\beta_2} & 0 & 0 & 0 & 0 & 0 \\
0 & 0 & 0 & 0 & 0 & 0 & 0 & 0 & 0 & 1 & 0 & 0 & 0 & 0 & 0 & 0 & 0 & 0 \\
0 & 0 & -\frac{\bar{c}_{21}}{\beta_2} & 0 & 0 & 0 & 0 & 0 & H_4 & 0 & 0 & 0 & 0 & 0 & -\frac{\bar{c}_{23}}{\beta_2} & 0 & 0 & 0 \\
0 & 0 & 0 & 0 & 0 & 0 & 0 & 0 & 0 & 0 & 0 & 1 & 0 & 0 & 0 & 0 & 0 & 0 \\
0 & 0 & 0 & 0 & -\frac{\bar{c}_{21}}{\beta_2} & 0 & 0 & 0 & 0 & 0 & K_2 & 0 & 0 & 0 & 0 & 0 & -\frac{\bar{c}_{23}}{\beta_2} & 0 \\
0 & 0 & 0 & 0 & 0 & 0 & 0 & 0 & 0 & 0 & 0 & 0 & 0 & 1 & 0 & 0 & 0 & 0 \\
-\frac{\bar{c}_{31}}{\beta_3} & 0 & 0 & 0 & 0 & 0 & -\frac{\bar{c}_{32}}{\beta_3} & 0 & 0 & 0 & 0 & 0 & H_5 & 0 & 0 & 0 & 0 & 0 \\
0 & 0 & 0 & 0 & 0 & 0 & 0 & 0 & 0 & 0 & 0 & 0 & 0 & 0 & 0 & 1 & 0 & 0 \\
0 & 0 & -\frac{\bar{c}_{31}}{\beta_3} & 0 & 0 & 0 & 0 & 0 & -\frac{\bar{c}_{32}}{\beta_3} & 0 & 0 & 0 & 0 & 0 & H_6 & 0 & 0 & 0 \\
0 & 0 & 0 & 0 & 0 & 0 & 0 & 0 & 0 & 0 & 0 & 0 & 0 & 0 & 0 & 0 & 0 & 1 \\
0 & 0 & 0 & 0 & -\frac{\bar{c}_{31}}{\beta_3} & 0 & 0 & 0 & 0 & 0 & -\frac{\bar{c}_{32}}{\beta_3} & 0 & 0 & 0 & 0 & 0 & K_3 & 0
\end{bmatrix} \tag{16}$$

where

$$K_1 = -(\lambda_3^4 + u^2 d_{33} - \bar{c}_{12} - \bar{c}_{13}), \quad K_2 = -\frac{1}{\beta_2}(\lambda_3^4 - \bar{c}_{21} - \bar{c}_{23}), \quad K_3 = -\frac{1}{\beta_3}(\lambda_3^4 - \bar{c}_{31} - \bar{c}_{32}). \tag{17}$$

Thus, the characteristic equation of the system of Eqs. (13) and (16) are stated as

$$\det(\lambda[I] - [C]) = 0, \tag{18}$$

where $[I]$ is an identity matrix.

3. Results and discussions

The fluid-conveyed TWCNTs are analyzed to determine the instability characteristics and the influences of the vdW interactions between the different nanotubes. In numerical computations, the TWCNTs considered are clamped at both ends. The inner, middle and outer tubes have the same length L, and they are modeled by using Euler-beam model. The initial separation between two adjacent tubes is taken as 0.34 nm. The parameters that are used in calculating the vdW interactions coefficient are $\varepsilon = 2.968$ meV, $a = 1.42$ Å and $\sigma = 3.407$ Å [28]. The tubes have the same Young's modulus $E = 1$ TPa with the mass density 2.3 g/cm^3, and the mass density of water 1 g/cm^3. In order to examine the influences of the radii of the TWCNTs, two cases are considered. The first case is the inner radius $R_1 = 3.4$ nm which is about 20 water molecular sizes

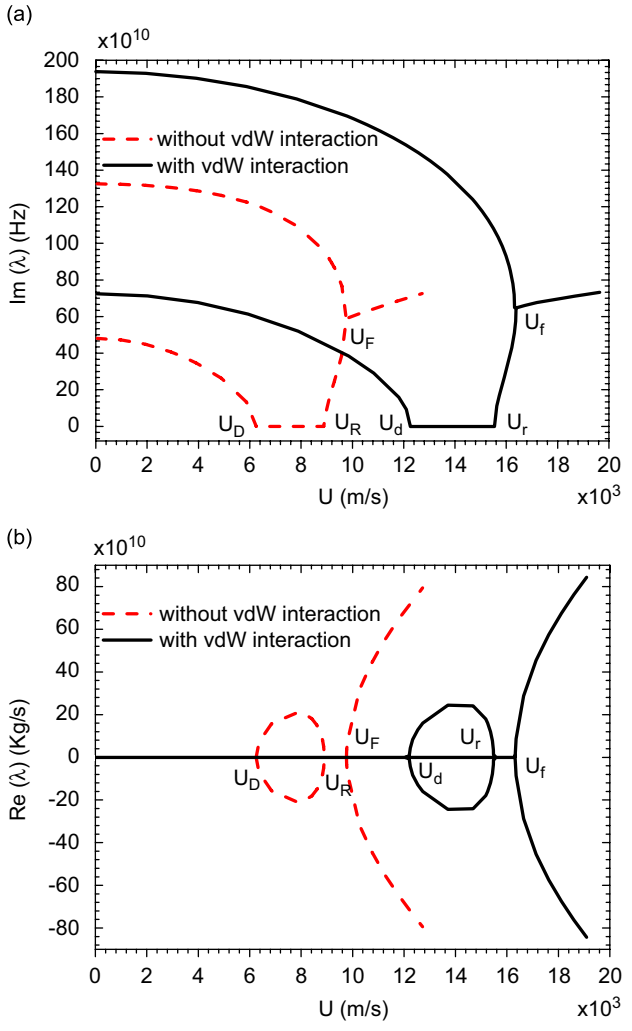

Fig. 2. Evolution of the imaginary and real parts of eigenvalues λ with increasing velocity U when $N = 2$, $R_1 = 3.4$ nm and $L/R_2 = 10$.

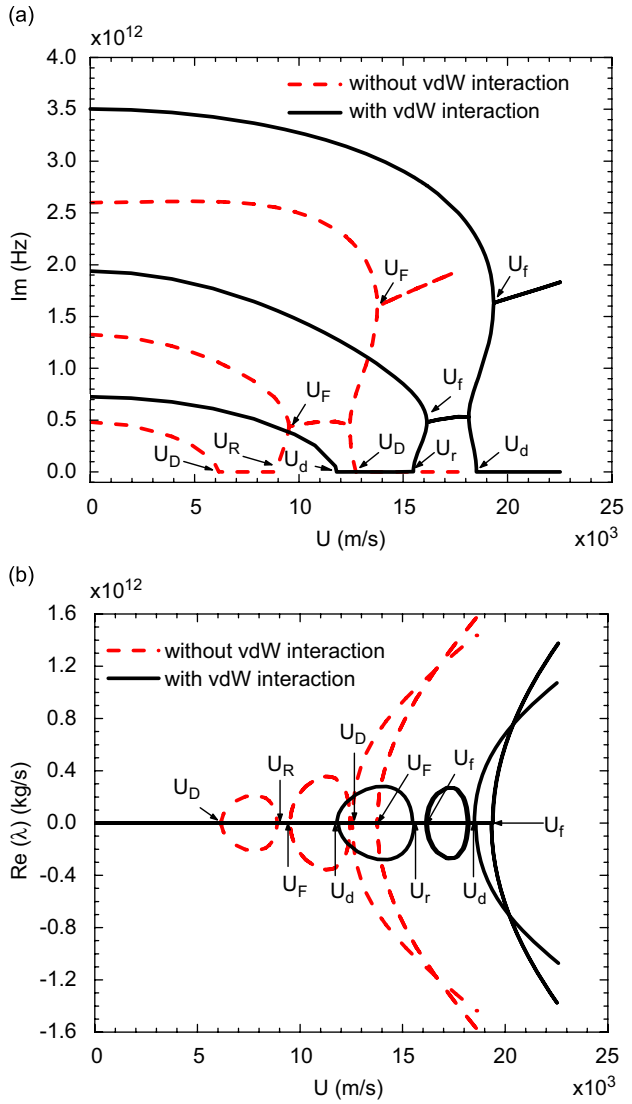

Fig. 3. Evolution of imaginary and real parts of eigenvalue with velocity U for $N = 3$, $R_1 = 3.4$ nm and $L/R_2 = 10$.

(the middle radius $R_2 = 3.74$ nm and the outer radius $R_3 = 4.08$ nm), and the second case the inner radius of $R_1 = 11.9$ nm which is about 79 water molecular sizes (the middle radius $R_2 = 12.24$ nm and the outer radius $R_3 = 12.58$ nm). Because the radii used in the analysis are larger than 1 nm and the number of the water molecules in the tube is more than 10, so it makes sure that the continuum model predictions are valuable. Moreover, something about flow velocity should be mentioned that the available data in the literature for flow velocity inside CNTs range from 400 m/s [30] to 2000 m/s [6], or even up to 50,000 m/s [31].

Mathematically, the evolution of a system towards divergence or flutter may be tracked by plotting the complex eigenvalues in the plane [32]. The diagrams for the evolution of the real and imaginary parts of the eigenvalues of the CNTs conveying fluid are plotted as the function of the fluid velocity U in Figs. 2–5 for the cases $R_1 = 3.4$ and 11.9 nm, namely $N = 2$ and 3, respectively. Figs. 2a to 5a show the dependency of the imaginary part of the eigenvalues (which represent the natural frequencies) of the inner CNT as the fluid velocity, and Figs. 2b to 5b are the plottings of the real part of the eigenvalue which is regarded as a "damping mechanism" resulting from the flow energy transfer from the moving fluid to the inner wall of the TWCNTs.

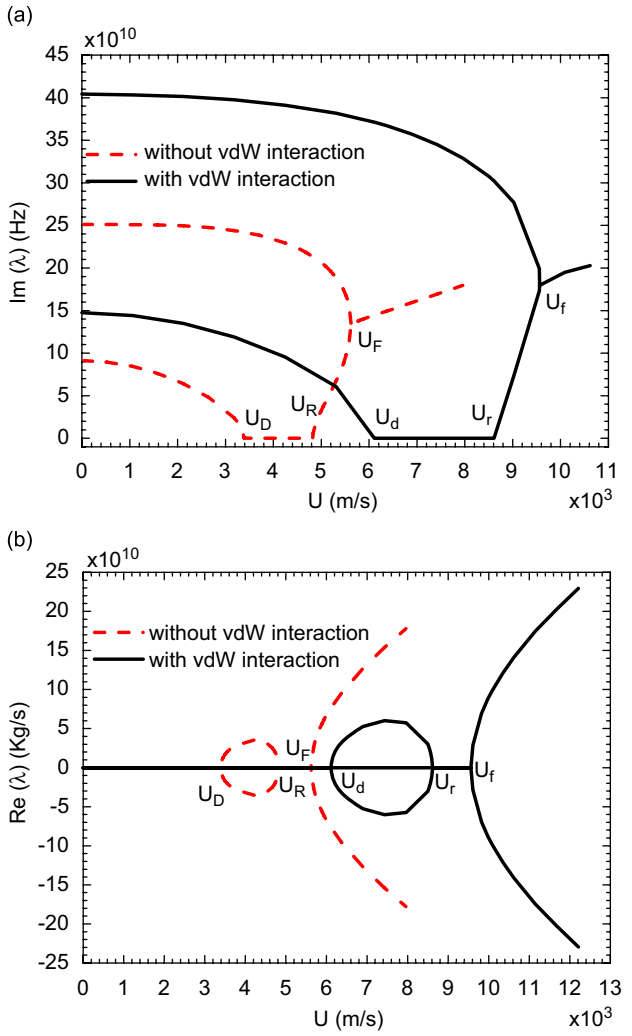

Fig. 4. Evolution of the imaginary and real parts of eigenvalues λ with increasing velocity U when $N = 2$, $R_1 = 11.9$ nm and $L/R_2 = 10$.

The real part is positive for the unstable TWCNTs as the fluid velocity, or negative for the stable characteristics.

The critical flow velocities of the system are identified sequentially by U_D, U_R and U_F without the vdW interactions and by U_d, U_r and U_f with the vdW interactions. As a typical dynamic behavior example, Fig. 2 is taken to examine the influences of the fluid on the instabilities of the fluid-conveyed TWCNTs. The results show that the internal moving fluid significantly affects the natural frequencies of the inner tube. In the case with vdW interactions, in the region of $U < U_d$ the two different frequency curves decrease parabolically with increasing fluid velocities, and the real parts of all eigenvalues are zero, as shown in Fig. 2b. These imply that the system is stable. While when the first critical velocity U_d is reached, the natural frequency of the first mode becomes zero, which the system loses its stability due to the divergence via a pitchfork bifurcation. Thereafter, in the region of $U_d < U < U_r$, the eigenvalues have the positive real parts, which the system becomes unstable. When the velocity is in the region of $U \geqslant U_r$, the imaginary parts of all eigenvalues are distinguished and the real parts become zero, as shown in Figs. 2a, b. This implies that the critical velocity U_r does not correspond to the unstable state and the system restabilizes until $U = U_f$, whereupon the loci of the first and second modes coalesce at point U_f, as shown in Fig. 2a, which indicates the onset of the flutter via a

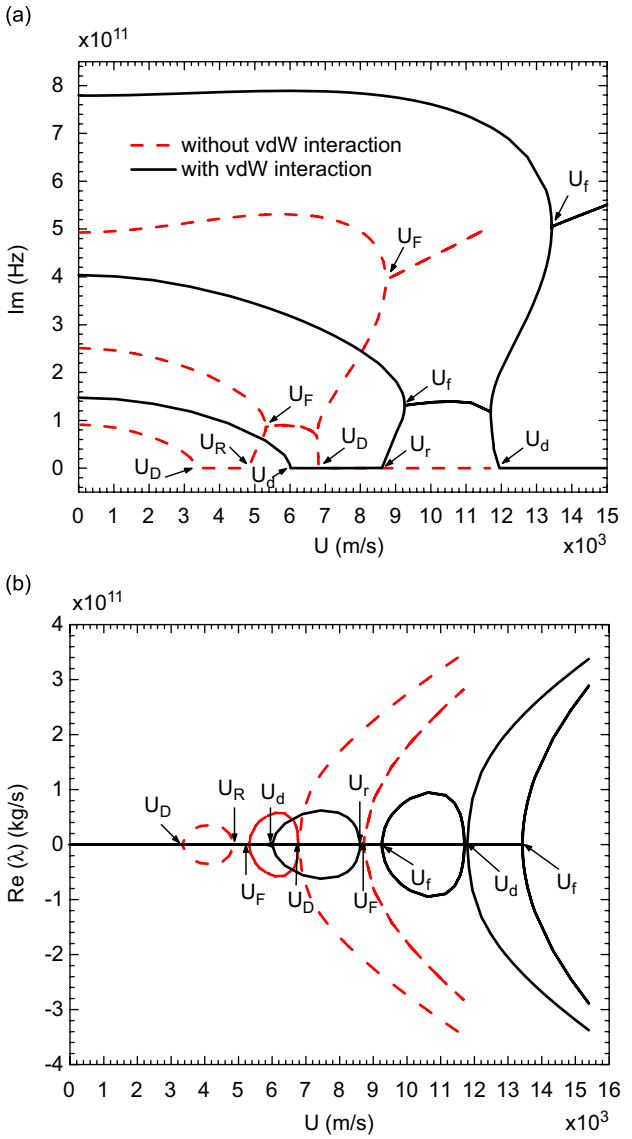

Fig. 5. Evolution of imaginary and real parts of eigenvalue with velocity U for $N = 3$, $R_1 = 11.9\,\text{nm}$ and $L/R_2 = 10$.

Hamiltonian Hopf bifurcation. After $U > U_f$, as one of the real part is positive, the system becomes unstable once more.

Next, we discuss the influence of the vdW interaction. Considering a TWCNT conveying fluid without vdW interaction, we have $c_{ij} = 0$. In this case, Eqs. (7a)–(7c) are reduced to a common beam model. It is evident from Figs. 2 to 5 that the values of the critical velocities are decreased. This shows that the system is more stable with vdW interactions. So, the vdW interactions benefit improvement of the system stability. For the effects of the inner tube radius and length-to-middle radius on the stability, the changes of the critical velocities are listed in Table 1 and shown in Figs. 6 and 7 with the length-to-middle radius ratios L/R_2. It is observed from Table 1 and Figs. 6 and 7 that the critical velocities of the system are dependent on the inner radius. The smaller is the inner radius, the higher is the critical velocities. The reason is explained as Ref. [21] that the flexural restoring force of a smaller radius CNT is significantly larger than that of a larger radius CNT. Thus, the interactions between the fluid and the inner tube wall have to resist the restoring force of the

Table 1
Critical flow velocity for the instability of the inner tube (m/s)

Critical velocity U	With vdW interaction $L/R_2 = 10$		Without vdW interaction $L/R_2 = 10$	
	$N = 2$	$N = 3$	$N = 2$	$N = 3$
3.4 nm				
Divergence	12,106	12,106	6247	6247
Restabilization	15,482	15,482	8896	8896
Flutter	16,325	16,128	9763	9521
Divergence	–	18,506	–	12,593
Flutter	–	19,332	–	13,758
11.9 nm				
Divergence	6110	6110	3387	3387
Restabilization	8611	8611	4823	4823
Flutter	9563	9264	5622	5521
Divergence	–	11,839	–	6916
Flutter	–	13,432	–	8733

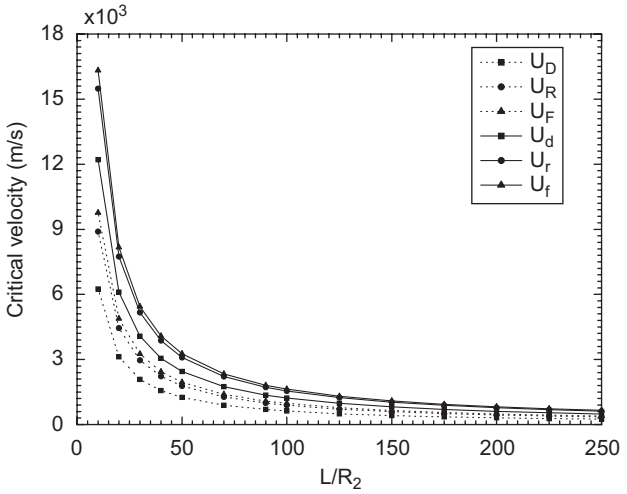

Fig. 6. Critical velocities with $R_1 = 3.4$ nm for $N = 2$ of clamped TWCNTs.

smaller radius CNTs at a higher flow velocity. However, for TWCNTs with the same radius, the critical velocities are relatively high for small length-to-middle radius ratios. The critical velocities decrease sharply as the length-to-middle radius ratio increases for $L/R_2 \leqslant 50$, and then vary slowly as the flow velocity and tend to a constant value when the length-to-middle radius ratio is large enough.

To examine the effect of fluid flow inside the inner tube on the instability of the middle and outer tubes, the natural frequencies of TWCNTs with various inner radii are calculated and listed in Table 2 for various fluid velocities. It can be seen that the variation of natural frequencies is very small and can be neglected. This indicates that fluid flow has very little influence on the dynamic characteristics of the middle tube and outer tube. In addition, it is observed that the vdW interaction plays an important role in the natural frequencies of the middle and the outer tube.

Finally, we discuss the effects of the different terms N in the Galerkin approximation on the stability. If we take more terms (>2) in the approximation solutions in Eq. (10), the matrix $[C]$ become more complex, for example, when $N = 2$, it is a 12×12 matrix; when $N = 3$, it is a 18×18 matrix; and when $N = 4$, it is a

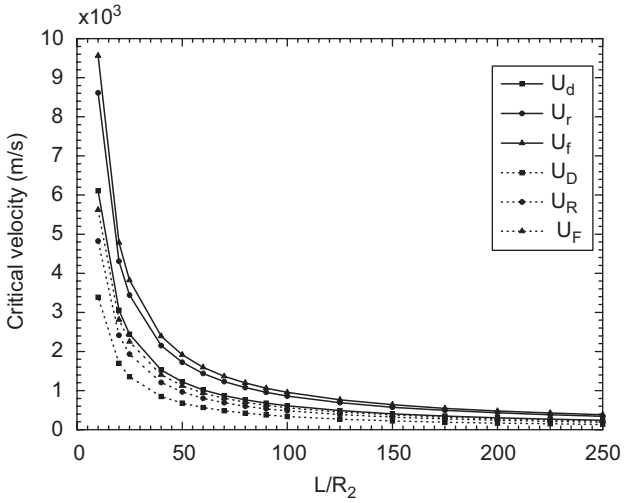

Fig. 7. Critical velocities with $R_1 = 11.9$ nm for $N = 2$ of clamped TWCNTs.

Table 2
Natural frequencies ($\times 10^{10}$ Hz) of the middle tube and outer tube

Inner radius R_1	Velocity U (km/s)	With vdW interaction $L/R_2 = 10$					Without vdW interaction $L/R_2 = 10$				
		$N = 2$		$N = 3$			$N = 2$		$N = 3$		
		Mode 1	Mode 2	Mode 1	Mode 2	Mode 3	Mode 1	Mode 2	Mode 1	Mode 2	Mode 3
3.4 nm	Middle tube										
	0	498.14	544.60	498.14	544.60	689.34	92.30	254.22	92.30	254.22	498.78
	2.65	497.71	544.96	497.84	545.50	689.38	92.30	254.22	92.30	254.22	498.78
	5.30	496.50	545.97	496.57	549.24	689.62	92.30	254.22	92.30	254.22	498.78
	7.95	494.65	547.46	494.91	554.21	689.94	92.30	254.22	92.30	254.22	498.78
	10.6	492.42	549.20	492.93	559.99	690.35	92.30	254.22	92.30	254.22	498.78
	Outer tube										
	0	1074.12	1100.22	1074.06	1100.23	1182.55	100.30	276.28	100.30	276.28	542.06
	2.65	1074.12	1100.24	1074.06	1100.25	1182.55	100.30	276.28	100.30	276.28	542.06
	5.30	1074.08	1100.35	1074.04	1100.44	1182.55	100.30	276.28	100.30	276.28	542.06
	7.95	1074.07	1100.36	1074.04	1100.70	1182.59	100.30	276.28	100.30	276.28	542.06
	10.6	1074.06	1100.38	1074.02	1101.06	1182.61	100.30	276.28	100.30	276.28	542.06
11.9 nm	Middle tube										
	0	439.98	444.85	439.99	444.84	460.69	27.33	75.27	27.33	75.27	147.68
	2.65	439.74	445.10	439.75	445.00	460.89	27.33	75.27	27.33	75.27	147.68
	5.30	439.13	445.73	439.09	445.33	461.42	27.33	75.27	27.33	75.27	147.68
	7.95	438.33	446.57	438.24	445.69	462.36	27.33	75.27	27.33	75.27	147.68
	10.6	437.43	447.53	437.26	445.98	463.58	27.33	75.27	27.33	75.27	147.68
	Outer tube										
	0	1074.44	1076.72	1074.37	1076.65	1084.15	28.08	77.33	28.08	77.33	151.72
	2.65	1074.44	1076.72	1074.37	1076.65	1084.15	28.08	77.33	28.08	77.33	151.72
	5.30	1074.42	1076.74	1074.37	1076.69	1084.15	28.08	77.33	28.08	77.33	151.72
	7.95	1074.41	1076.76	1074.37	1076.69	1084.19	28.08	77.33	28.08	77.33	151.72
	10.6	1074.36	1076.76	1074.33	1076.73	1084.19	28.08	77.33	28.08	77.33	151.72

24×24 matrix. The comparisons of the evolution of the real and imaginary parts of the eigenvalues of the CNT-fluid system with $N = 2$ and 3 are plotted in Fig. 8 for $R_1 = 11.9$ nm and $L/R_2 = 50$ with vdW interactions. It is noted that with the increase of the terms N, the bifurcations of system become more complex.

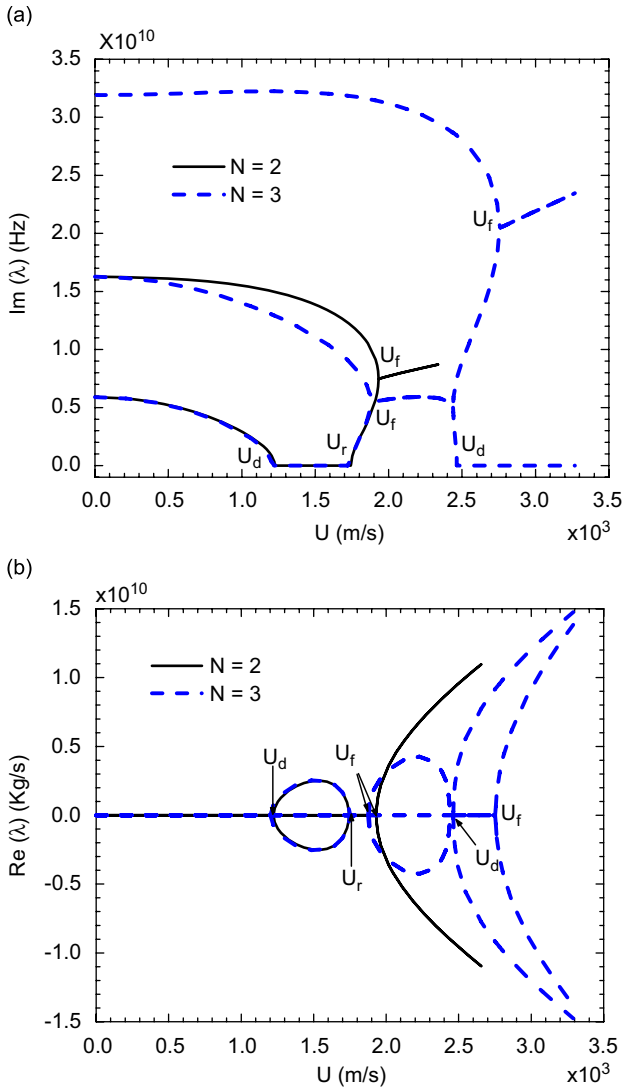

Fig. 8. Evolution of imaginary and real parts of eigenvalues λ with increasing velocity U when $R_1 = 11.9$ nm and $L/R_2 = 50$.

In general, high-N approximations become necessary to adequately represent the dynamics of the system as U is increased, where $N = 2$ Galerkin approximations can predict U_d or U_r very well.

4. Conclusions

The instability problems of the fluid-conveyed TWCNTs have been studied in this paper. The TWCNTs are modeled as Euler–Bernoulli beam. In contrast to the work by Yoon et al. [20,21], in which only the first critical flow velocity is determined for the instability of a SWCNT system, the critical flow velocities for the instabilities by a pitchfork bifurcation and a Hamiltonian Hopf bifurcation are obtained herein. The effects of the vdW interactions and the dimensions of TWCNTs on the stability are discussed, and the results show that the vdW interactions enhances the stability of the system, and the critical flow velocities increase very rapidly with decreasing inner radius. The internal moving fluid plays an important role in the instability of the CNTs-fluid system.

Acknowledgements

The work described in this paper is fully funded by a research grant from the Research Grants Council of the Hong Kong Special Administrative Region, China [Project No. CityU 113406]. The authors are grateful for this financial support.

References

[1] I. Hanasaki, A. Nakatani, Water flow through carbon nanotube junctions as molecular convergent nozzles, *Nanotechnology* 17 (2006) 2794–2804.
[2] R.J. Mashl, S. Joseph, N.R. Aluru, E. Jakobsson, Anomalously immobilized water: a new water phase induced by confinement in nanotubes, *Nano Letter* 3 (2003) 589–592.
[3] V.P. Sokhan, D. Nicholson, N. Quirke, J. Chem, Fluid flow in nanopores: an examination of hydrodynamic boundary conditions, *Journal of Chemical physics* 115 (2001) 3878–3887.
[4] T. Werder, J.H. Walther, R.L. Jaffe, T. Halicioglu, F. Noca, P. Koumoutsakos, Molecular dynamics simulation of contact angle of water droplet in carbon nanotubes, *Nano Letter* 1 (2001) 697–702.
[5] A. Skoulidas, D.M. Ackerman, K.J. Johnson, D.S. Sholl, Rapid transport of gases in CNTs, *Physical Review Letters* 89 (2002) 185901.
[6] R.E. Tuzun, D.W. Noid, B.G. Sumpter, R.C. Merkle, Dynamics of fluid flow inside CNTs, *Nanotechnology* 7 (1996) 241–246.
[7] G.D. Mahan, Oscillations of a thin hollow cylinder: carbon nanotubes, *Physical Review B* 65 (2002) 235402.
[8] A.M. Rao, J. Chen, E. Richter, U. Schlecht, P.C. Eklund, R.C. Haddon, U.D. Venkateswaran, Y.K. Kwon, D. Tomanek, Effect of van der Waals interactions on the Raman modes in single walled carbon nanotubes, *Physical Review Letters* 86 (2001) 3895.
[9] V.N. Popov, V.E. Van Doren, M. Balkanski, Elastic properties of single-walled carbon nanotubes, *Physical Review B* 61 (2000) 3078–3084.
[10] A. Garg, J. Han, S. Sinnott, Interactions of carbon-nanotubule proximal probe tips with diamond and grapheme, *Physical Review Letters* 81 (1998) 2260–2263.
[11] M.J. Treacy, T.W. Ebbesen, J.M. Gibson, Exceptionally high Young's modulus observed for individual carbon nanotubes, *Nature* 381 (1996) 678–800.
[12] P. Poncharal, Z.L. Wang, D. Ugarte, W.A. Heer, Electrostatic deflections and electromechanical resonances of carbon nanotubes, *Science* 283 (1999) 1513–1516.
[13] Y. Gogotsi, In situ multiphase fluid experiments in hydrothermal CNTs, *Applied Physical Letters* 79 (2001) 1021–1023.
[14] J.K. Holt, H.G. Park, Y.M. Wang, et al., Fast mass transport through sub-2 nanometer carbon nanotubes, *Science* 312 (2006) 1034–1037.
[15] K.P. Travis, D.J. Evans, Molecular spin in a fluid undergoing Poiseuille flow, *Physical Review E* 55 (1996) 1566–1572.
[16] J. Koplik, J.R. Bnavar, J.F. Willemsen, Molecular dynamics of fluid flow at solid surfaces, *Physics of Fluids A* 1 (1989) 781–794.
[17] L.A. Pozhar, Structure dynamics of nanofluids: theory and simulations to calculate viscosity, *Physical Review E* 61 (2000) 1432.
[18] K.P. Travis, K.E. Gubbins, Poiseuille flow of Lennard–Jones fluids in narrow slit pores, *Journal of Chemical physics* 112 (2000) 1984–1994.
[19] K.P. Travis, B.D. Todd, D.J. Evans, Departure from Navier–Stokes hydrodynamics in confined liquids, *Physical Review E* 55 (1997) 4288–4295.
[20] J. Yoon, C.Q. Ru, A. Mioduchowski, Vibration and instability of CNTs conveying fluid, *Composites Science and Technology* 65 (2005) 1326–1336.
[21] J. Yoon, C.Q. Ru, A. Mioduchowski, Flow-induced flutter instability of cantilever CNTs, *International Journal of Solids and Structures* 43 (2006) 3337–3349.
[22] J. Yoon, C.Q. Ru, A. Mioduchowski, Noncoaxial resonance of an isolated multiwall carbon nanotube, *Physical Review B* 66 (2002) 233402.
[23] J. Yoon, C.Q. Ru, A. Mioduchowski, Vibration of an embedded multiwall carbon nanotube, *Composites Science and Technology* 63 (2003) 1533–1542.
[24] C.Q. Ru, Elastic models for carbon nanotubes, in: H.S. Nalwa (Ed.), *Encyclopedia of Nanoscience and Nanotechnology*, Vol. 2, American Scientific, Stevenson Ranch, CA, 2004, pp. 731–744.
[25] T. Natsuki, Q.Q. Ni, M. Endo, Wave propagation in single- and double-walled carbon nanotubes filled with fluids, *Journal of Applied Physics* 101 (2007) 034319.
[26] Y. Yan, X.Q. He, L.X. Zhang, Q. Wang, Flow-induced instability of double-walled carbon nanotubes based on an elastic shell model, *Journal of Applied physics* 102 (2007) 044307.
[27] X.Q. He, S. Kitipornchai, K.M. Liew, Buckling analysis of multi-walled carbon nanotubes: a continuum model accounting for van der Waals interaction, *Journal of the Mechanics and Physics of Solids* 53 (2005) 303–326.
[28] R. Saito, R. Matsuo, T. Kimura, G. Dresselhaus, M.S. Dresselhaus, Anomalous potential barrier of double-wall carbon nanotube, *Chemical Physics Letters* 348 (2001) 187–193.
[29] L.X. Zhang, K. Yang, *The Theory and its Applications of Fluid-Structure Interaction*, Science Press, Beijing, 2004 (in Chinese).
[30] S. Supple, N. Quirke, Rapid imbibition of fluids in CNTs, *Physical Review Letters* 90 (2003) 214501.
[31] Z. Mao, S.B. Sinnott, A computational study of molecular diffusion and dynamics flow through CNTs, *Journal of Chemical Physics B* 104 (2000) 4618–4624.
[32] M.P. Paidoussis, *Fluid-Structure Interactions*, Vol. 1, Academic Press, San Diego, 1998.